CONF-950740--19

MODELING OF GRAIN BOUNDARY STRESSES IN ALLOY 600

Krzysztof J. Kozaczek
Oak Ridge National Laboratory
Oak Ridge, TN 37831-6064

Arindam Sinharoy and Clayton O. Ruud
The Pennsylvania State University
University Park, PA 16802

Allan R. McIlree
Electric Power Research Institute
Palo Alto, CA 94304-1395

ABSTRACT

Corrosive environments combined with high stress levels and susceptible microstructures can cause the intergranular stress corrosion cracking (IGSCC) of Alloy 600 components on both primary and secondary sides of pressurized water reactors. One of the factors affecting the IGSCC is the intergranular carbide precipitation controlled by the heat treatment of Alloy 600. The present study is concerned with the analysis of elastic stress fields in the vicinity of M_7C_3 and $M_{23}C_6$ carbides precipitated in the matrix and at a grain boundary triple point. The local stress concentration which can lead to IGSCC initiation was studied using a two-dimensional finite element model. The intergranular precipitates are more effective stress raisers than the intragranular precipitates. The combination of the elastic property mismatch and the precipitate shape can result in a local stress field substantially different than the macroscopic stress. The maximum local stresses in the vicinity of the intergranular precipitate were almost twice as high as the applied stress.

INTRODUCTION

Alloy 600 is a solid solution nickel-based alloy (Ni-15Cr-10Fe and with other minor alloying additives) which is widely used for steam generator tubing, control rod drive and pressurizer nozzles in nuclear power plants. Corrosive environments combined with high stress levels and "susceptible" microstructure cause the intergranular stress corrosion cracking (IGSCC) of Alloy 600 components. Particular examples are the steam generator heat exchanger tubing for nuclear power plants on both primary and secondary sides (outside and inside diameter surfaces). In the past two decades the grain boundary chemistry, grain size, and intergranular and matrix carbide phase precipitation have been studied extensively in relation to IGSCC [1-18]. The role of the grain boundary carbides in the process of intergranular fracture is not yet fully understood. Experimental results show that depending upon the carbide morphology and volume fraction, and the type of corrosive environment, the effect on the IGSCC susceptibility is either beneficial, detrimental or neutral.

A mechanical theory proposed by Bruemmer and Henager [12,13] explained the effect of carbides on IGSCC in terms of microdeformation mechanisms. The interface between the matrix grain boundary and the carbides is the principal source of dislocations. Dislocation motion is initiated at grain boundary carbides and grain boundary intersections (triple points). Second-phase particles are a good source of dislocations because of the presence of an elastic discontinuity at the particle-matrix interface. Localized stress relief by microplastic deformation is more homogeneous where a large number of second-phase particles exist, and leads

to more uniform distribution of strains in grain boundary regions.

The present study is concerned with the analysis of elastic stress fields in the vicinity of second-phase particles precipitated either in the grain interior or at the grain boundary triple point. Residual stresses due to the thermal expansion coefficient mismatch are not considered. It is the elastic stress concentration at a second-phase particle which can lead to the local microplastic deformation and in consequence influence the IGSCC susceptibility of the alloy.

MODELING OF CARBIDE PRECIPITATES

Carbide morphology

The morphology of carbide precipitates is relatively well documented. The grain boundary precipitates in solution annealed and heat treated Alloy 600 are predominantly a mixture of M_7C_3 and $M_{23}C_6$ with neither of these two carbides clearly dominant [1,15-16]. Four classes of the grain boundary carbide precipitate morphology were reported: fine discrete particles, semicontinuous precipitates, coarse semicontinuous precipitates, and large discrete precipitates [1, 8-10, 18]. The average precipitate size and density depend on the heat treatment [9,13]. The observed range of the average discrete precipitate length was from 1 to 3 μm, and the average distance between precipitates was 0.7 to 2.5 μm [9].

Carbides of the M_7C_3 type have a hexagonal crystal structure and hardness of 236 HV [9, 19]. The crystal structure of $M_{23}X_6$ (X is non-metallic) is face centered cubic [9, 20].

There is no reported data on the orientation relationships between $M_{23}C_6$ and Cr_7C_3 and the matrix in Alloy 600. However, the mechanism of formation and growth of $M_{23}C_6$ carbides in austenite have been reported [21-25]. The carbides nucleate with longer axes parallel to <110> of the austenite within the boundary plane. The carbides are in parallel orientation with one of the matrix grains at a triple point and create a high-angle grain boundary with other grains. At longer aging times the carbides are embedded in the matrix of the grain with which they are in parallel orientation as a result of the grain boundary migration. Grain boundary triple points are very favorable sites for massive $M_{23}C_6$ formation. The information regarding the mechanism of formation and orientation relationships with the matrix for carbides of the M_7C_3 type is not available in the literature.

The single crystal elastic constants and thermal expansion coefficients for M_7C_3 and $M_{23}C_6$ carbides are not available. Elastic moduli for a Fe_3C carbide were cited as E=268 GPa and ν=0.28 [26] (E is Young's modulus, ν is Poisson's ratio). The moduli reported for carbide ceramics are much higher (e.g., for silicon carbide E=430 GPa, for boron carbide E=430 GPa, for tungsten carbide E=605 GPa [27]). In general, the precipitates have a higher stiffness than the metal matrix.

Two-dimensional finite element model

Based upon the carbide-matrix relationship discussed in the previous section, a model of a second-phase particle at the grain boundary triple point is proposed (Figure 1). The second-phase particle is in parallel orientation with grain A in the figure. The grain boundaries are assumed to be of <001> type. The grain orientations were selected as Φ_A=0°, Φ_B=45°, and Φ_C=22.5° since they provide for the maximum elastic mismatch between the grains [28]. Grains A and B have, therefore, a disorientation of 45° with the grain boundary plane parallel to the (100) plane of grain A. Grain boundaries A-C and B-C have a 22.5° disorientation and are close to the (110) planes of grain C and (010) planes of grain B, respectively. The condition for the $M_{23}C_6$ carbide growth is therefore satisfied since the A-C interface is a (110) plane. Also the "egg-shaped" carbide is embedded into grain A with which it is in parallel orientation. The disorientation angle of 45° is close to the most probable disorientation angle (mean disorientation angle is 40.74°) between grains in a random polycrystal [29].

The finite element model contained 2519 nodes and 836 eight-node quadrilateral elements (Figure 1). Meshing was done using the Patran preprocessor, and the finite element analysis was done with the ABAQUS package. The stress tensor invariants (i.e., von Mises stress and hydrostatic pressure) were requested as the output since they are relevant to the theories of crack initiation. The hydrostatic pressure is defined as $\sigma_m=\sigma_{ii}/3$, von Mises stress $\sigma'=\sigma_{ij} \cdot \sigma_m\delta_{ij}$, where σ_{ij} is the stress tensor and δ is the Kronecker's delta. The external load was applied by defining the displacements on the top and right edges of the system in such a way that the resultant average normal stress on each loaded edge was equal to 1.0 (arbitrary units).

By changing the orientation of grains two cases were studied: a carbide embedded in a grain (intragranular precipitate) and a carbide precipitated at the grain boundary triple point.

Precipitate embedded in anisotropic matrix

The anisotropic elastic properties were assigned with all three grains having the same orientation ([001] direction parallel to the horizontal direction in Fig.1) simulating therefore an inclusion embedded in a single grain or in a highly textured material. The single crystal elastic properties of Alloy 600 were used (C_{11}=232 GPa, C_{12}=148 GPa, C_{44}=115.9 GPa which translates to approximately E=200 GPa and ν=0.3 [31]). The precipitate was simulated as having a high stiffness i.e., E=400 GPa, ν=0.1. The system was loaded in equi-biaxial tension (plane stress condition). The von Mises and hydrostatic stress fields are shown in Figure 2 (hydrostatic pressure is defined to be positive when it acts towards the surface upon which it is applied).

As seen in Fig.2 the applied load is supported mostly by the inclusion. Both the hydrostatic pressure and von Mises stresses have the highest concentration factor inside the inclusion K_c=1.22. The von Mises stress field inside the inclusion is not uniform. The highest stresses in the matrix are observed at the location where the grain boundary intersects the precipitate and at the highest curvature of the precipitate. The stress concentration in the matrix is relatively low, K_c=1.08.

Precipitate at grain boundary triple point

Grains A, B, and C were assigned the orientations 0, 45, and 22.5° respectively and the single crystal elastic constants of Alloy 600 (C_{11}=232 GPa, C_{12}=148 GPa, C_{44}=115.9 GPa [31]). The precipitate was assigned the elastic modulus E=400 GPa and Poisson's ratio ν=0.1 representing therefore a hard carbide particle. The effects of the stress state, i.e. uniaxial vs. equi-biaxial loading were studied. The analysis of residual stresses in Alloy 600 components (residual stresses due to manufacturing are much higher than applied stress) showed that those two states of stress, i.e. uniaxial and equi-biaxial, can be considered as "typical" [32-33]. The stress fields for the uniaxial load are shown in Fig.3, for the equi-biaxial load in Fig.4. When the system is loaded in the uniaxial mode (Fig.3) the hydrostatic pressure in the matrix shows a variation from tensile to compressive with a stress concentration factor of K_c=1.97 and the ratio of the maximum to minimum stresses $\sigma_{max}/\sigma_{min}$=-15.5. The stress field is aligned with the direction of the applied load and the maximum stresses occur at the precipitate/matrix interface. The stress concentration factor for the von Mises stress in the matrix is K_c=1.67. The von Mises stress variation in the matrix is $\sigma_{max}/\sigma_{min}$=3.65. Both the von Mises stress and the hydrostatic pressure are concentrated along the boundary between grains A and C. The stress fields inside the inclusion are not uniform. The stress fields due to the equi-biaxial loading (Fig.4) are more uniform. The highest hydrostatic pressure occurs inside the inclusion (K_c=1.23). In the matrix the hydrostatic pressure is concentrated along the grain boundaries (K_c=1.05). The von Mises stress is highest inside the inclusion (K_c=1.26) with some concentration in the matrix along the grain boundaries (K_c=1.1).

CONCLUSIONS

Elastic stresses in the grain boundary regions caused by the elastic properties mismatch between a carbide precipitate and a nickel alloy matrix were studied by finite element modeling. The effects of precipitate location i.e., intragranular vs. intergranular, and external stress state on the stress fields around the precipitate were analyzed. An intragranular carbide precipitate is not as effective a stress raiser as a carbide precipitated at a grain boundary triple point due to the contributing effect of strain incompatibilities between the grains in the latter case. The precipitate with the effective elastic modulus higher than that for the surrounding grains (which is the case for all types of carbides present in stainless steels and nickel based alloys) supports more load than the matrix, i.e. the stresses inside the precipitate are higher than in the alloy grains. The shape of the inclusion plays a role in the stress distribution in the grain boundary regions; sharp corners raise stresses more effectively than oblong-shaped precipitates. Equi-biaxial loading provides for a more uniform distribution of stresses than uniaxial loading. The high stress fields are confined to the vicinity of the grain boundary precipitate (their range is much smaller than the size of the precipitate) and therefore for the large spaced grain boundary carbides their elastic interactions are insignificant. For Alloy 600 the highest stress concentration factors observed were

K_C=1.97 for the hydrostatic pressure and K_C=1.67 for the von Mises stress and were caused by the uniaxial loading applied along the longer axis of the precipitate. Thus, the tip of the precipitate where those concentrations occur is the favorable place for the initiation of microplastic deformation.

ACKNOWLEDGMENTS

Research sponsored by EPRI under contract RP2812-13 and partially (KJK) by the U. S. Department of Energy, Assistant Secretary for Energy Efficiency and Renewable Energy, Office of Transportation Technologies, as part of the High Temperature Materials Laboratory User Program under contract DE-AC05-84OR21400, managed by Martin Marietta Energy Systems, Inc.

REFERENCES

1. G.P. AIREY, "Microstructural Aspects of the Thermal Treatment of Inconel Alloy 600," *Metallography* **13** (1980) 21.
2. G.P. AIREY and A.R. VAIA, "A Caustic Stress-Corrosion Cracking Evaluation of Thermally Treated Inconel Alloy 600 Steam Generator Tubing," MiCon 82: Optimization of Processing Properties and Service Performance Through Microstructural Control," edited by H. Abrams, E. Clark, J. Hood, B. Seth (ASTM, Philadelphia, 1982) p. 59.
3. EPRI Report No NP-5072 ,"Specially Prepared Alloy 600 Tubing," 1987.
4. K. NORRING, J. ENGSTROM, and P. NORBERG, in Proc. Third International Symposium on Environmental Degradation of Materials in Nuclear Power Systems - Water Reactors (TMS-AIME, Warrendale, PA, 1988) p.587.
5. G.S. WAS, "Grain Boundary Chemistry and Intergranular Fracture in Austenitic Nickel-Base Alloys--A Review," *Corrosion* 46(4) (1990) 319.
6. EPRI Report No TR-101983, "Characterization of Microstructure and IGSCC of Alloy 600 Steam Genarator Tubing," 1993.
7. X. LIU, J. SHAO, and D.D. MACDONALD, "Corrosion of Nickel-Base Alloys," ed. by R.C. SCARBERRY (ASM International, Materials Park, OH, 1985) p.211.
8. M. KOWAKA, H. NAGANO, T. KUDO, Y. OKADA, et al., "Effect of Heat Treatment on the Susceptibility to Stress Corrosion Cracking of Alloy 600," *Nuclear Technology* **55** (Nov. 1981) 394.
9. J.J. KAI, C.H. TSAI, T.A. HUANG, and M.N. LIU, "The Effects of Heat Treatment on the Sensitization and SCC Behavior of Inconel 600 Alloy," *Metal. Trans. A* **20A** (June 1989) 1077.
10. G.S. WAS, J.K. SUNG, and T.M. ANGELU, "Effects of Grain Boundary Chemistry on the Intergranular Cracking Behavior of Ni-16Cr-9Fe in High-Temperature Water," *Metall. Transactions A*, **23A** (Dec. 1992) 3343.
11. J.K. SUNG, J. KOCH, T. ANGELU, and G.S. WAS, "The Effect of Grain Boundary Chemistry on Intergranular Stress Corrosion Cracking of Ni-Cr-Fe Alloys in 50 Pct. NaOH at 140°C," *Metall. Transactions A*, **23A** (October 1992) 2887.
12. S.M. BRUEMMER and C.H. HENAGER, JR., "High Voltage Electron Microscopy Observations of Microdeformation in Alloy 600 Tubing," *Scripta Metall.* **20** (1986) 909.
13. S.M. BRUEMMER, L.A. CHARLOT, and C.H. HENAGER, JR., "Microstructure and Microdeformation Effects on IGSCC of Alloy 600 Steam Generator Tubing," *Corrosion* 44(11) (1988) 782.
14. S.M. BRUEMMER, "Interfacial Precipitation, Segragation and Deformation in Alloy 600: Implications on Primary Side IGSCC," presented at EPRI Alloy 600 Expert Meeting, Airlie, VA, 6-9 April 1993.
15. E.L. HALL, and C.L. BRIANT, " The Microstructure Response of Mill-Annealed and Solution-Annealed Inconel 600 to Heat Treatment," *Metall. Transactions A* **16A** (July 1985) 1225.
16. G.S. WAS, and R.M. KRUGER, "A Thermodynamic and Kinetic Basis for Understanding Chromium Depletion in Ni-Cr-Fe Alloys," *Acta Metall.* 33(5) (1985) 841.
17. R.M. KRUGER, G.S. WAS, J.F. MANSFIELD, and J.R. MARTIN, "A Quantitative Model for the Intergranular Precipitation of M_7X_3 and $M_{23}X_6$ in Ni-16Cr-9Fe-C-B," *Acta Metall.* 36(12) (1988) 3163.
18. R. BANDY, and D. VAN ROOYEN, "Mechanisms of Stress Corrosion Cracking and Intergranular Attack in Alloy 600 in High Temperature Caustic and Pure

Water," *J. Mat. Energy Systems* **7**(3) (Dec.1985) 237.
19. D.J. DYSON, and K.W. ANDREWS, "Carbide M_7C_3 and its formation in Alloy Steels," *J. Iron and Steel Institute* **207** (Feb. 1969) 208.
20. A.L. BOWMAN,G.P. ARNOLD,E.K. STORMS, and N.G. NERESON, "The Crystal Structure of $Cr_{23}C_6$," *Acta Crystall.* **B28** (1972) 3102.
21. L.K. SINGHAL, and J.W. MARTIN, "The Growth of $M_{23}C_6$ Carbide on Grain Boundaries in an Austenitic Stainless Steel," *Trans. Metall. Soc. AIME* **242** (May 1968) 814.
22. U.E. WOLFF, "Orientation and Morphology of $M_{23}C_6$ Precipitated in High-Nickel Austenite," *Trans. Metall. Soc. AIME* **236** (Jan. 1966) 19.
23. M.H. LEWIS, and B. HATTERSLEY, "Precipitation of $M_{23}C_6$ in Austenitic Steels," *Acta Metall.* **13** (nov. 1965) 1159.
24. F.R. BECKITT, and B.R. CLARK, "The Shape and Mechanism of Formation of $M_{23}C_6$ Carbide in Austenite," *Acta Metall.* **15** (Jan. 1967) 113.
25. T.F. LIU, S.W. PENG, Y.L. LIN, and C.C. WU, "Orientation Relationships among $M_{23}C_6$, M_6C, and Austenite in an Fe-Mn-Al-Mo-C Alloy," *Metall. Transactions A* **21A** (March 1990) 567.
26. S.H. GOODS et al. *Acta Metallurgica* **27** (1979) 1.
27. Norton, Northboro R&D Center, Northboro, MA.
28. K. KURZYDLOWSKI, Z. CELINSKI, and M.W. GRABSKI, "Finite Element Analysis of Conditions for Dislocation Generation on Grain Boundaries in Anisotropic Tricrystals under Tension," *Res. Mechanica* **1** (1980) 283.
29. J.D. ESHELBY, "The Detrmination of the Elastic Field of an Ellipsoidal Inclusion and Related Problems," *Proc. Roy. Soc.*, **A241** (1957) 376-396.
30. J.K. MACKENZIE, "Second Paper on Statistics Associated with the Random Disorientation of Cubes," *Biometrika* **45** (1958) 229.
31. K.J. KOZACZEK, B.G. PETROVIC, C.O. RUUD, S.K. KURTZ, A.R. MCILREE, "Microstructural Modeling of Grain Boundary Stresses in Alloy 600," *Journal of Materials Science* (in print).
32. C.O. RUUD et al. "Residual stresses in Roller Expanded Heat Exchanger Tube Transitions," EPRI Report, 1993.
33. C.O. RUUD et al. "Residual Stress Analysis of Alloy 600 U-Bends, RUBs, and C-Rings, EPRI Report, 1991.

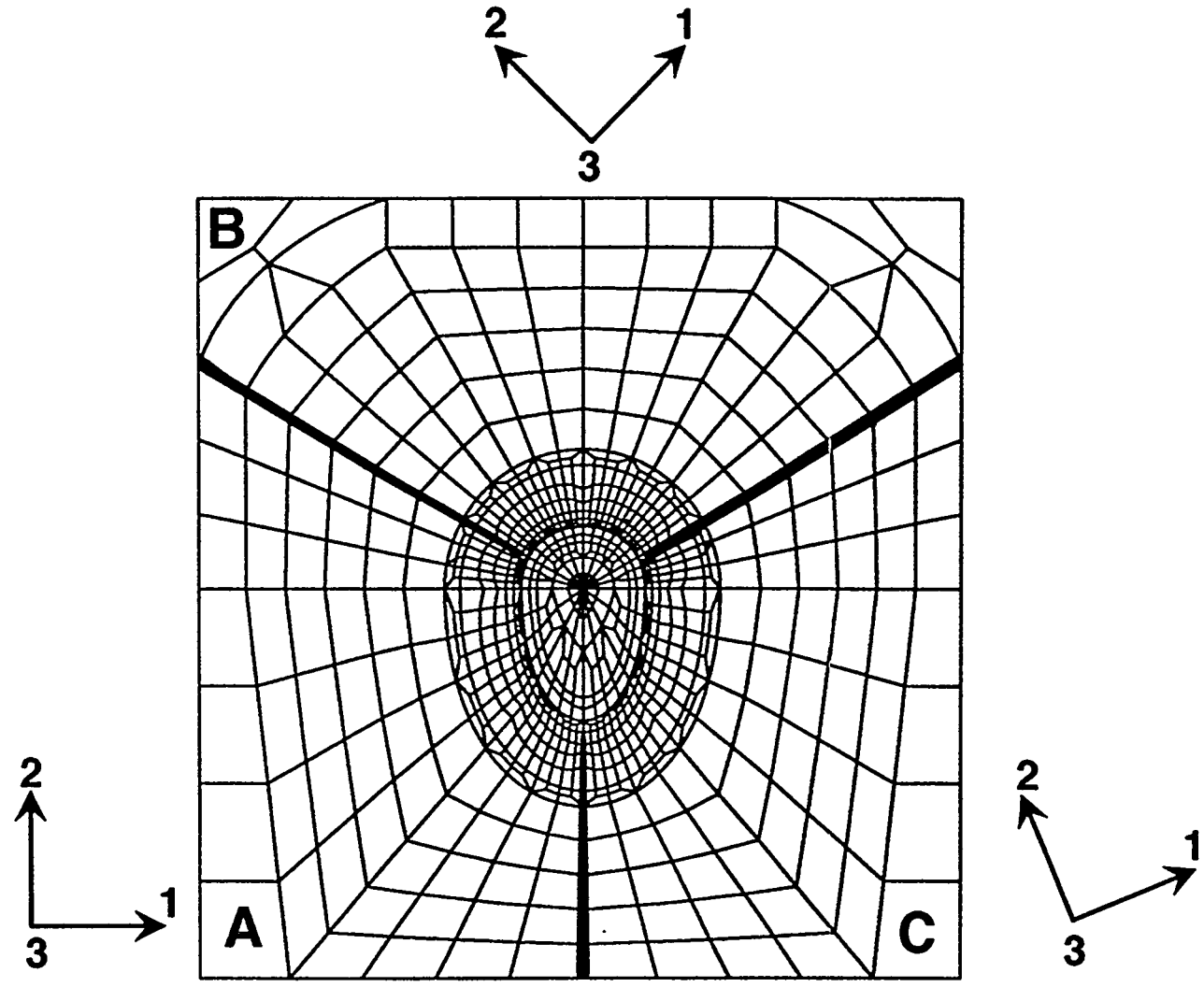

FIGURE 1. MODEL OF CARBIDE PRECIPITATE AT GRAIN BOUNDARY TRIPLE POINT

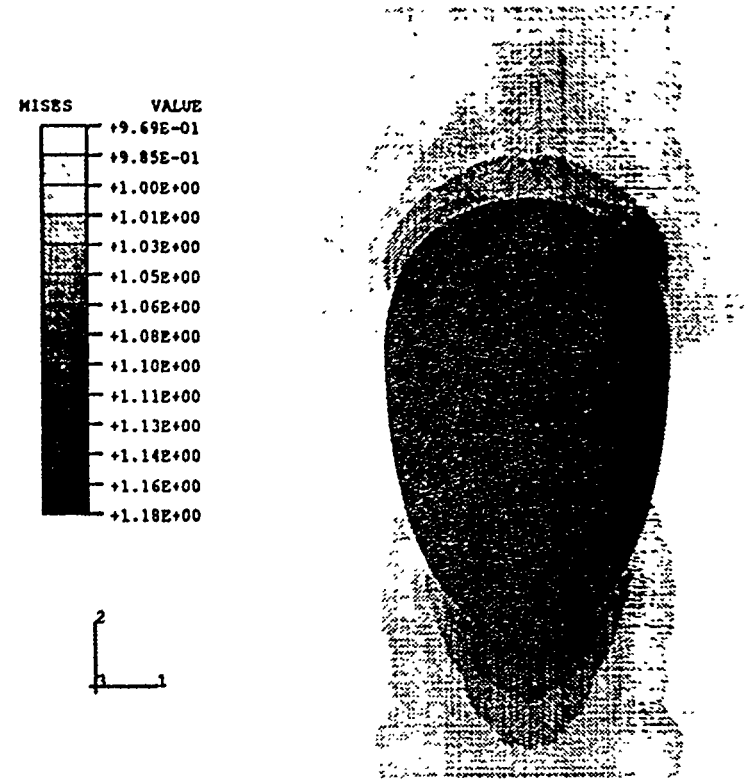

A

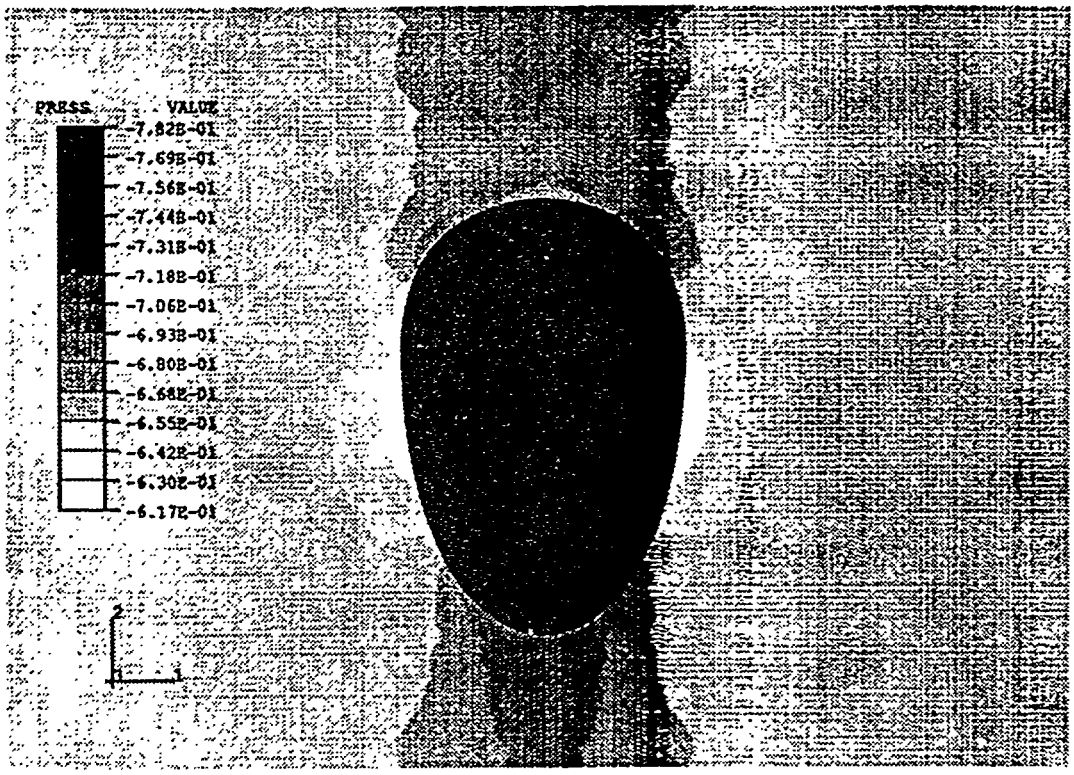

B

FIGURE 2. VON MISES STRESS (A) AND HYDROSTATIC PRESSURE (B) FIELDS AROUND AN INTRAGRANULAR CARBIDE PRECIPITATE

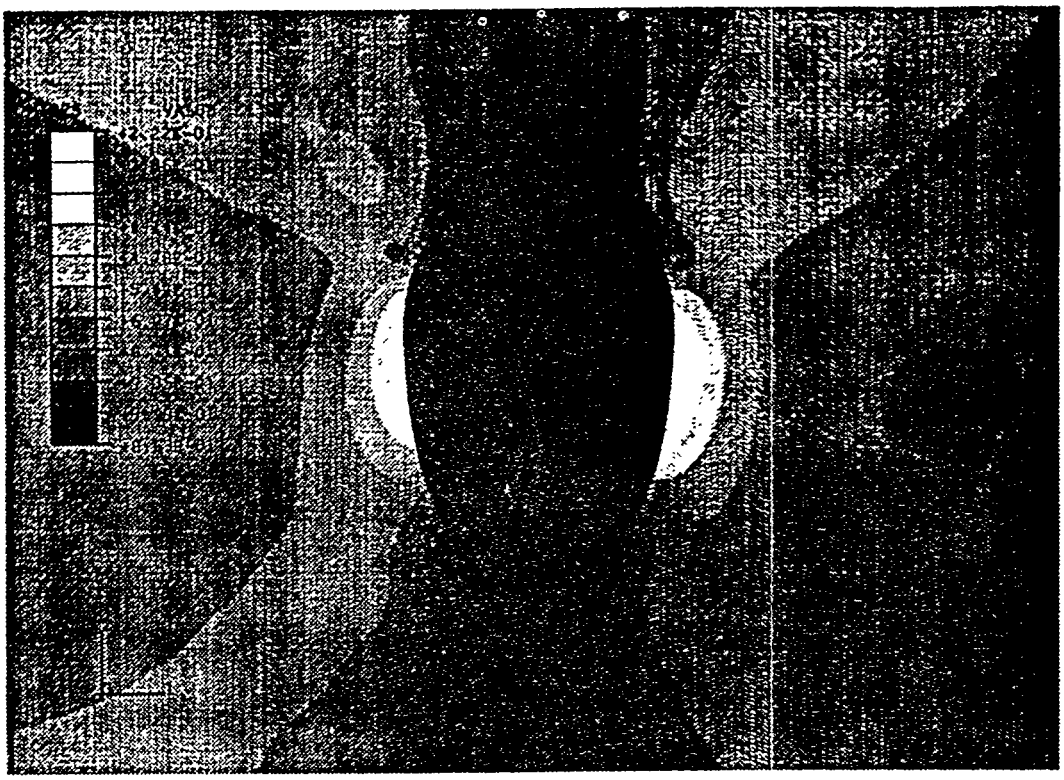

A

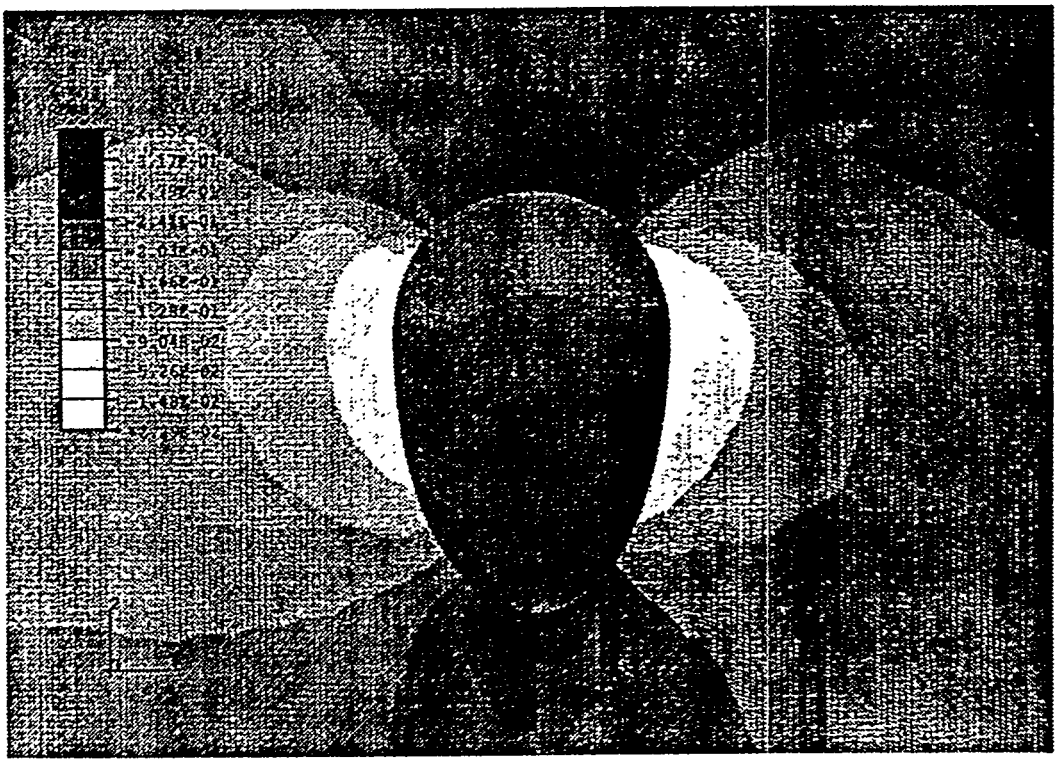

B

FIGURE 3. VON MISES STRESS (A) AND HYDROSTATIC PRESSURE (B) AROUND A CARBIDE PRECIPITATE AT GRAIN BOUNDARY DUE TO UNIAXIAL TENSION

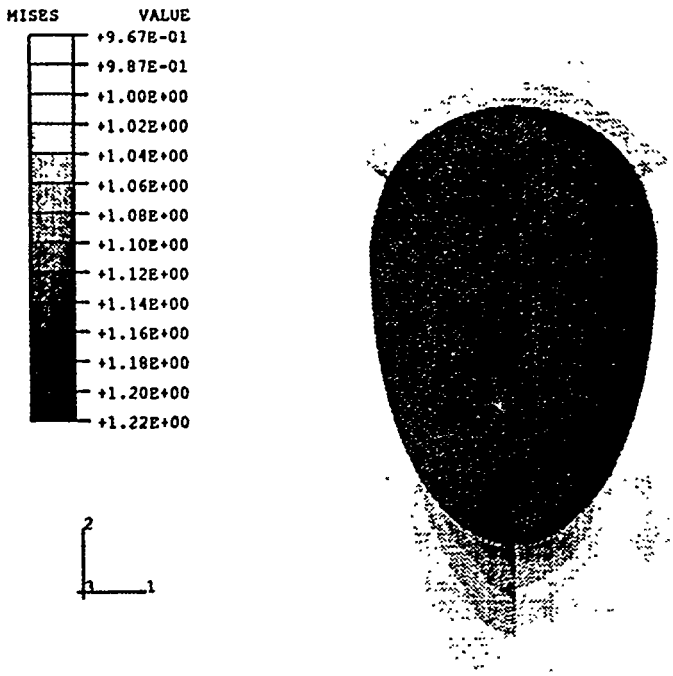

A

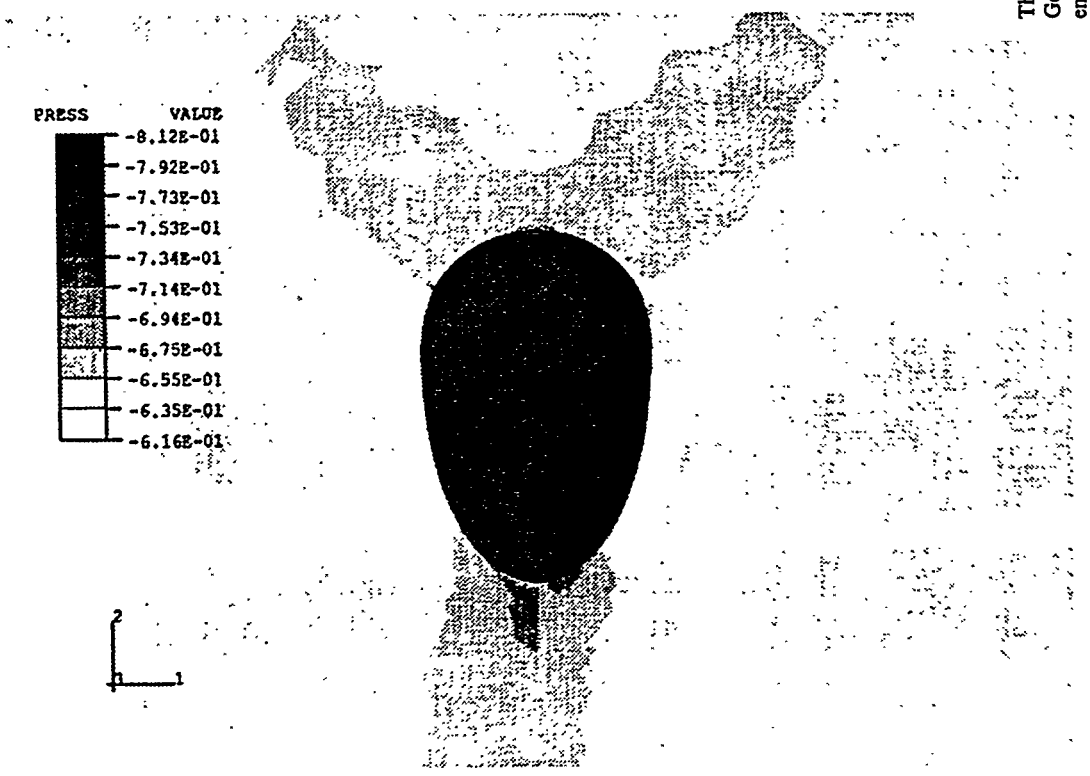

B

FIGURE 4. VON MISES STRESS (A) AND HYDROSTATIC PRESSURE (B) AROUND A CARBIDE PRECIPITATE AT GRAIN BOUNDARY DUE TO EQUI-BIAXIAL TENSION